Mineralogical Magazine (2019), **83**, 249–260
doi:10.1180/mgm.2018.165

CAMBRIDGE UNIVERSITY PRESS

Article

Geochemistry of pink corundum-bearing feldspathic gneiss, Frenchvale quarry, Cape Breton Island, Canada: metamorphism of albitised, Fe-poor clastic rocks

J. Victor Owen[1]*, Jacob J. Hanley[1], Mitchell J. Kerr[1], Matthew Stimson[1] and Brandon Boucher[2]

[1]Department of Geology, Saint Mary's University, Halifax, Nova Scotia, Canada B3H 3C3; and [2]Dept. of Earth Sciences, University of New Brunswick, Fredericton, New Brunswick, Canada

Abstract

Frenchvale quarry, once mined for dolomitic marble, contains pink corundum-bearing, quartz-free/-poor, feldspathic gneiss that is unusually sodic (~7% wt.% Na_2O) and iron-poor (~0.6 wt.% Fe_2O_3), but has silica, alumina and immobile trace-element contents resembling those of suspended fluvial particulate matter (e.g. in the Congo River). The protolith of the gneiss, interpreted as a fine-grained clastic sediment deposited offshore, evidently was albitised prior to deformation and regional metamorphism. Variably-altered gneiss samples show a narrow range of $\delta^{18}O_{VSMOW}$ values (8.1 to 10.7‰) and no systematic differences in bulk O isotope composition as a function of alteration intensity. With the exception of an extensively fuchsitised zone adjacent to a thick (1.2 m), cross-cutting quartz vein that contains H_2O–NaCl+CO_2+CH_4-bearing fluid inclusions, the O isotope data do not support interaction of the gneiss with an externally-derived fluid phase except at low fluid:rock ratio, even where granodiorite occurs in direct contact with the gneiss. Fluid inclusions in the quartz vein have bulk X_{H_2O}, X_{CO_2} and X_{CH_4} values (in mol.%) of 99.60, 0.14 and 0.26, respectively, as determined by gas chromatography. Although the protolith of the gneiss was associated with carbonate platformal rocks (now marble), corundum is confined to the feldspathic rocks. These feldspathic rocks lack calc-silicate minerals; they are not skarns. As such, they are distinct from well-known Himalayan sapphire and ruby deposits cited previously as analogues of the Frenchvale corundum occurrence.

(Received 11 December 2017; accepted 4 October 2018)

Introduction

Pink sapphire and ruby (Cr-bearing corundum) are known from a variety of geological settings. The principal economic deposits of this mineral can be subdivided into two main categories (Giuliani *et al.*, 2014): (1) magmatic deposits hosted by mafic/ultramafic rocks associated with granitoid rocks and hydrothermal activity (Type 1A), or by alkali basalts and mafic dykes (Type 1B); and (2) metamorphic deposits hosted by marine sediments from a carbonate platform (Type 2). The largest known single occurrence of these gemstones is a Type 1A occurrence: the Aappaluttoq deposit of southwestern Greenland. It formed in a contact zone between ultramafic rocks and metagabbro in the Archean Fiskenaesset anorthosite (Fagan and Groat, 2014). Elsewhere in Greenland, ruby occurs in metasomatised aluminosilicate-bearing aluminous gneiss in contact with amphibole-peridotite (Yakymchuk and Szilas, 2017. The corundum in Type 1B deposits occurs as xenocrysts in the alkali basalt flows, or as megacrysts in xenoliths. Notable examples occur in Thailand and Australia (e.g. Levinson and Cook, 1994; Sutherland *et al.*, 1998). Some of the world's best known and most productive pink sapphire and ruby deposits are hosted by metacarbonate/calc-silicate rocks (Type 2 deposits). Of these, the most prominent occur in the southern Himalaya. In some of these metacarbonate-hosted deposits, the coloured corundum is interpreted to have formed by the mobilisation of fluids along narrow shear zones cutting dolomitic marble (Pêcher *et al.*, 2002), but elsewhere, ruby occurs in calcite-bearing marble associated with high-grade metapelites cut by granitoid rocks (Okrusch *et al.*, 1976). Some of the highest quality, carbonate-hosted gem corundum deposits, in Myanmar, have a trace-element signature (V, Ti, Cr) indicating geochemical contributions from black shales associated with the platformal carbonate rocks (Harlow and Bender, 2013).

There are Canadian examples of carbonate-hosted gem corundum deposits, near Revelstoke, British Columbia, and Kimmirut, Nunavut (Dzikowski 2004). A recently-discovered low-grade, coloured (pink to lilac) corundum occurrence in Cape Breton (Nova Scotia, Canada) has been described as sharing elements of the geological setting of some of the Himalayan deposits, particularly those in the Hunza region of Gilgit-Baltistan, northern Pakistan (Mossman *et al.*, 2007). This present paper uses field data, microstructural features, bulk-rock and mineralogical compositional data, bulk-rock oxygen isotopes and fluid-inclusion compositions to shed light on the petrogenesis of the Cape Breton corundum occurrence.

Field occurrence

Corundum-bearing feldspathic gneiss associated with dolomitic marble is exposed in a 0.6 km long quarry near Frenchvale,

***Author for correspondence:** J. Victor Owen, Email: victor.owen@smu.ca
Associate Editor: Craig Storey
Cite this article: Owen J.V., Hanley J.J., Kerr M.J., Stimson M. and Boucher B. (2019) Geochemistry of pink corundum-bearing feldspathic gneiss, Frenchvale quarry, Cape Breton Island, Canada: metamorphism of albitised, Fe-poor clastic rocks. *Mineralogical Magazine* **83**, 249–260. https://doi.org/10.1180/mgm.2018.165

Cape Breton Island (Fig. 1, inset map). We found no younging direction indicators to show whether the feldspathic gneiss is older or younger than the dolomitic marble that structurally underlies it. These rocks, and subordinate metapelites and metapsammites that crop out elsewhere in the area, are part of the Frenchvale Road metamorphic suite, one of several low-pressure, late Proterozoic inliers belonging to the Bras d'Or gneiss/metamorphic suite as defined by Raeside (1989) and Raeside and Barr, 1990) that crop out near the southeastern margin of the Bras d'Or terrane (Fig. 1, inset map). The Bras d'Or terrane is characterised by younger granitoid rocks (565–555 Ma) than those (*c.* 620 Ma) in the adjacent Mira terrane to the south that are interpreted to have been generated in a separate volcanic arc (Barr, 1990). The boundary between these terranes is structurally complex (King and Barr, 2002), and, based on the age of intrusive rocks (see below) in the Frenchvale quarry, evidently occurs farther south than indicated by Raeside and Barr (1990; see Fig. 1, inset map).

The metacarbonates include relatively pure, white dolomitic marble as well as millimetre-scale bands – probably relict bedding – containing diopside, serpentinised forsterite and/or tremolite and/or wollastonite. The metapelites found elsewhere in the Bras d'Or gneiss include biotite + muscovite + sillimanite- and cordierite + sillimanite + andalusite-bearing variants. Raeside (1989) noted that garnet, where present, appears to be metastable relative to cordierite. This implies that the cordierite formed at the expense of garnet during decompression of the Bras d'Or gneiss. Raeside (1989) used a petrogenetic grid to infer peak metamorphic temperatures for these rocks in excess of 600°C at a pressure of 3.0–4.5 kbar.

The paragneisses at Frenchvale quarry host metre- to decametre-scale sheets of fine-grained biotite ± hornblende granodiorite and granitic pegmatite. Contacts with the host rocks are poorly exposed in the quarry, but in places are seen to be discordant with respect to gneissosity (Mossman *et al.*, 2007). Both the feldspathic gneiss and the granitoid rocks locally contain greenschist-facies assemblages related to a late, passive sericitisation and chloritisation overprint. Given the preservation of discordant igneous contacts, low-grade partial retrogression of amphibolite-facies assemblages in the gneisses is therefore interpreted to post-date emplacement of the granodiorite and pegmatite. The granodiorite has yielded a preliminary U–Pb (zircon) age of 560 Ma (Hopkins *et al.*, 2017), indicating that the Frenchvale quarry rocks are part of the Bras d'Or terrane. Similar intrusive ages (550–565 Ma) were reported for syn- and post-tectonic plutons cutting gneissic rocks in the Creignish Hills, in the southwestern part of the Bras d'Or terrane (White *et al.*, 2016) (Fig. 1 inset map). Detrital zircons in some of the metasedimentary host rocks of these plutons indicate depositional ages of ≤600 Ma, indicating the rapid transformation from a passive to Andean continental margin during the late Neoproterozoic. The age of metamorphic rocks in the Bras d'Or terrane is constrained poorly; radiometric age determination of a tonalite dyke thought on petrographic grounds to be relatively old and therefore likely to provide a better constraint on the minimum age of its metamorphic host rocks nonetheless yielded a U–Pb (zircon) age of 564 ± 5.1 Ma (Barr *et al.*, 1999). Available age determinations therefore indicate that the protolith of the feldspathic gneiss was deposited, lithified, deformed and metamorphosed in the upper amphibolite facies, and intruded by felsic intrusive rocks, between ~600 and 560 Ma.

A sketch map of the quarry by Mossman *et al.* (2007) suggests that the corundum tends to be associated spatially with the granodiorite, but Mossman *et al.* interpreted the paragneisses as having been "altered" during regional (rather than contact) metamorphism, and described them (p. 280) as being "skarn, or more specifically, 'skarnoid rocks' ". Their map (Mossman *et al.*, 2007, p. 281) does not specifically identify or distinguish the feldspathic gneiss described here; the metamorphic rocks in the quarry are described as "Precambrian skarn and marble" implying that all the gneissic rocks are metacarbonate rocks. Moreover, Mossman *et al.* (2007, p. 284) described these rocks as "siliceous corundum-bearing marble" and in this regard likens them to Hunza Valley gem deposits. Similarly, Hopkins *et al.* (2017) described this occurrence as a skarn deposit, and they describe the corundum as occurring in a wollastonite, calcite, dolomite and quartz matrix. Skarns, however, are generally interpreted as being formed during the hydrothermal alteration of carbonate or calc-silicate rocks near plutons, and the term 'skarnoid' refers to calc-silicate rocks that are lithologically intermediate between "purely metamorphic hornfels" and a "purely metasomatic coarse-grained skarn" (Meinert, 1992, p.146). Although associated spatially with dolomitic marble, our samples of corundum-bearing feldspathic gneiss from Frenchvale quarry lack calc-silicate minerals and no carbonate minerals other than a single, narrow (~1 mm) calcite vein cutting one sample of this rock. Corundum was not identified in the dolomitic marble. Consequently, we avoid using the terms 'skarn' and 'skarnoid' to describe the corundum-bearing rocks from this locality, and refer to them instead as feldspathic gneiss.

Gneissosity and lithological layering both dip moderately (35–40°) to the northwest, implying the transposition of the primary foliation during deformation. A steeply southwest-dipping (75°), 1.2 m wide quartz vein cuts the corundum-bearing rocks in the northeastern part of the quarry where samples for the present investigation were collected (Fig. 1). Field observations suggest that the quartz vein was emplaced in a shear zone with a predominately dip-slip displacement component. These observations include: (1) the presence of pseudotachylite associated spatially with this structure; (2) the development of shallow-plunging drag folds in adjacent dolomitic marble; (3) the transposition of gneissic fabrics adjacent to the quartz vein; and (4) the occurrence of steeply northwest- to southeast-plunging mineral lineations (including slickenlines) adjacent to the quartz vein. Some of the nearby gneissic rocks are very dark owing to the presence of graphite. Gneissic fabrics in the part of the quarry we sampled have consistently moderate northwest dips, showing that faulting has not substantially modified their orientation except close to the quartz vein, where tectonic and lithological layering is transposed.

Corundum is altered variably to bright green fuchsite up to ~17 m to the southwest of the quartz vein; fuchsitisation is most intense within a few metres of this feature. The development of fracture cleavage developed on both (upper and lower) contacts of a 6 m thick granodiorite sheet west-southwest of the quartz vein (Fig. 1) suggests that this particular intrusive contact has been faulted (i.e. it is a faulted intrusive contact). No corundum was observed in the feldspathic gneiss structurally below the granodiorite. Rusty (relatively sulfide-rich) feldspathic gneiss immediately to the east-northeast of the quartz vein (Fig. 1) was not sampled, but corundum was noted in it.

Analytical methods

Representative samples of the various lithologies from Frenchvale quarry were powdered in preparation for bulk-rock analysis by

https://doi.org/10.1180/mgm.2018.165 Published online by Cambridge University Press

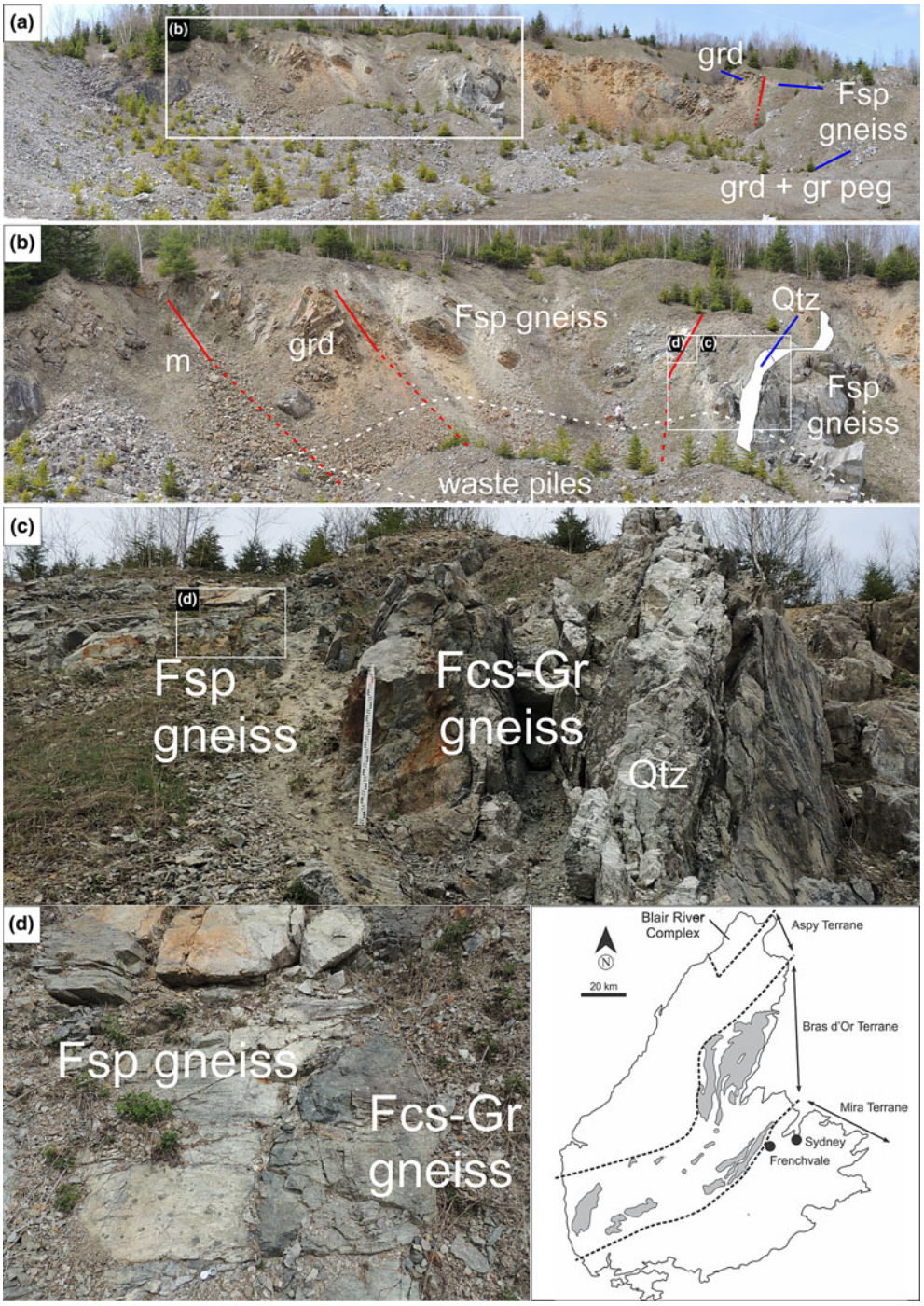

Fig. 1. Annotated composite photograph of part of Frenchvale quarry viewed looking towards the NNW. Successive rectangular insets highlight parts of the outcrop in increasing detail. Abbreviations: Fsp gneiss = feldspathic gneiss; Fcs-Gr gneiss = fuchsitised-graphite-bearing feldspathic gneiss; m = marble; grd = granodiorite; gr peg = granitic pegmatite; and Qtz = quartz vein. Red lines highlight geological contacts; lines are dashed where extrapolated across poor exposure. Inset map showing terranes in Cape Breton Island is after Raeside and Barr (1990). On the basis of the age of granodiorite in the quarry, the boundary between the Bras d'Or and Mira terranes should be farther south than shown here.

inductively coupled plasma optical emission spectrometry (ICP-OES) (major and minor elements) and inductively coupled plasma mass spectrometry (ICP-MS) (trace elements). Powders were prepared for analysis by lithium metaborate/tetraborate fusion followed by dilute nitric acid digestion (major/minor and selected trace elements). A separate split of 0.5 g of powder was digested by *aqua regia* for determination of base and precious metals. Polished thin sections were prepared using diamond pastes on glass and cloth laps. Mineral analyses were undertaken using: (1) a scanning electron microscope (SEM) equipped with an energy-dispersive spectrometer; and (2) for micas, an electron microprobe. The SEM used is a LEO 1450VP SEM operated with a beam current of 20 kV, and equipped with an Oxford Instrument INCA X-max 80 mm^2, silicon-drift EDS detector.

https://doi.org/10.1180/mgm.2018.165 Published online by Cambridge University Press

The SEM was also used to collect back-scattered electron images (BEI). The microprobe used is a JEOL8200 Superprobe equipped with five wavelength-dispersive spectrometers (WDS) and one energy-dispersive spectrometer (EDS). Analyses were performed using the WDS system. The operating voltage was 15 kV; beam current was 12 nA. Count time was 40 s. Probe current was measured with a Faraday cage. Detection limits for major and minor elements heavier than fluorine is in the order of 0.02–0.03 wt.% (cf. Dunham and Wilkinson, 1978). Standards included: jadeite (for Al, Si, Na); hornblende (Ca, Fe, Mg, Ti); sanidine (K); and apatite (P). Microprobe boron data for the dravite were imprecise, so this mineral, together with corundum, white mica and fuchsite, were analysed for trace elements (notably Cr) by laser ablation-ICP-MS at the University of New Brunswick. Aluminium (determined by SEM/EDS) was used as an internal standard.

Selected samples of each lithology, including the quartz vein, were analysed for oxygen isotopes at the Queen's University Facility for Isotope Research (Kingston, Canada). Owing to the prevalence of carbonate rocks at Frenchvale quarry, as a precaution, all dominantly silicate rock sample powders were acid washed to remove any carbonate minerals present. Oxygen was extracted from 5 mg samples at 550–600°C according to the conventional BrF_5 procedure of Clayton and Mayeda (1963) and analysed via a dual inlet on a Thermo-Finnigan DeltaPlus XP Isotope-Ratio Mass Spectrometer (IRMS). Silicate samples were reacted with BrF_5 to liberate O_2. This was converted to CO_2, and analysed in the mass spectrometer against a CO_2 reference gas calibrated against the Vienna Standard Mean Ocean Water (VSMOW) international standard. The mean of eight CO_2 measurements is reported for each sample. For corundum-bearing samples, finer grain sized material and longer reaction times are required to promote complete reaction. The $\delta^{18}O$ values are reported using the delta (δ) notation in units of per mil (‰) relative to VSMOW. A routine analytical precision of ±0.25‰ (1σ) was determined on the basis of repeated ($n = 10$ aliquots) analyses of the certified reference standard NBS28 (NIST 8546; silica sand). Bulk yields were typical for whole-rock isotope analysis, ranging between 12.7 and 16.3% (theoretical yield for a pure quartz sample is 16.65%).

Fluid-inclusion analyses were performed using a Linkham FTIR600 heating-freezing stage mounted on an Olympus BX51 microscope. Two fluid-inclusion sections were prepared from vein sample FQ29 for microthermometric analysis. Microthermometric uncertainties are ±0.2°C at a heating rate of 1°C/min. The 'fluid inclusion assemblage' criteria of Roedder (1984), Goldstein and Reynolds (1994) and Bodnar (2003) were used where applicable; however, significant decrepitation and the extremely small (<6 μm) nature of most inclusions made microthermometric analysis on fluid-inclusion assemblages extremely challenging. Most inclusions were too small to detect phase changes during heating-freezing experiments, so analysis was performed on any fluid inclusions sufficiently large to allow accurate measurement.

In situ laser Raman microspectroscopy was performed to determine the volatile composition of selected fluid inclusions in the quartz vein. Analysis was performed using a Horiba Jobin-Yvon LabRam HR confocal instrument equipped with a 100 mW, 532 nm, Nd-YAG diode laser (Toptica Photonics) and a Synapse charge-coupled device (CCD; Horiba Jobin-Yvon) detector. Pure silicon was used as a frequency calibration standard, and a 600 grooves/mm grating was used for the identification and quantification of fluid-inclusion-hosted volatiles. Semi-quantitative determination of these volatile species (in mol.%) was performed based on the methodology and parameters described by Wopenka and Pasteris (1986, 1987), Dubessy *et al.* (1989), Burke (2001) and Beeskow *et al.* (2005). In the absence of appropriate nitrogen standards, the instrumental efficiency factor was assumed to be unity resulting in the overestimation of molar abundance. Thus, the molar abundance of nitrogen is considered to represent a maximum.

The bulk composition of the quartz-hosted volatile fluid, trapped within fluid inclusions, was performed using an in-line rock/mineral-crushing gas chromatograph (GC; Bray and Spooner, 1992; Salvi and Williams-Jones, 1997; Kerr *et al.*, 2015). Sample material was crushed in a pre-cleaned, heated stainless steel hydraulic crusher from which trapped volatiles are liberated. Sample crushers pass liberated volatiles into an Agilent 7890 series gas chromatograph, adapted with appropriate valve and injection systems by Wasson-ECE Instrumentation for separation and quantification. An alumina-PLOT analytical column (30 m x 0.53 mm x 10 μm) was used in series with a thermal conductivity detector (TCD) and flame ionization detector (FID). Ultrapure helium carrier gas was set to a flow rate of 6.7 ± 0.5 ml/min. Sample crushing was carried out at elevated temperature (~105–110°C) in order to ensure that volatilisation of all entrapped fluids was achieved upon crushing. Calibration and identification of volatile species was performed using standard gas mixtures (Grace Davison Discovery Sciences).

Petrography and mineral compositions

The corundum-bearing gneiss is a feldspathic rock containing albite, alkali feldspar, white mica, rutile and (locally) dravite, with minor amounts of biotite, chlorite, monazite-(Ce), zircon and apatite. Corundum occurs as: (1) small (<1 mm long), partly corroded crystals (Fig. 2*a*), in places enclosed by fabric-forming muscovite (Fig. 2*e*); and (2) large (to 4 cm long), barrel-shaped porphyroblasts (Figs. 2*b*,*c*). Both occurrences can occur in the same sample, with the small corundum crystals being associated with more highly strained parts of the rock, whereas the barrel corundum porphyroblasts evidently have partitioned shear strain around them. Barrel corundum crystals nevertheless can be enveloped (or cut) by muscovite (Fig. 2*d*). Quartz is absent except as an accessory phase in highly altered (fuchsitised) samples. Foliation is defined predominantly by discontinuous bands and septae of fine-grained white mica ± chlorite ± biotite that occur in, or are separated by, relatively feldspathic layers and patches, some of which are lozenge-shaped. The small, partly corroded corundum crystals also define this fabric, as do trails of rutile, a conspicuous minor mineral in the rock that in places is associated with relict, variably chloritised, fabric-forming biotite, and occurs as inclusions in barrel corundum (Fig. 2*d*, *f*). The identity of rutile was confirmed by Raman spectroscopy (Fig. 3*a*). Preliminary age determination suggests that at least some of the rutile is coeval with the granodiorite, implying a contact metamorphic imprint on the feldspathic gneiss (Hopkins *et al.*, 2017). The gneissosity wraps around the barrel corundum crystals, and rinds of muscovite enclosing them commonly forms tails in pressure shadows adjacent to these porphyroblasts (Fig. 2*c*), further indicating a pre-kinematic origin of the corundum.

Dravite forms: (1) large (to 1.5 cm), elongated, brown to reddish brown porphyroblasts; and (2) small (to 1.5 mm), idiomorphic, equant, red crystals (Fig. 2*g*). The identity of the red dravite was confirmed by SEM/EDS and Raman spectroscopy

https://doi.org/10.1180/mgm.2018.165 Published online by Cambridge University Press

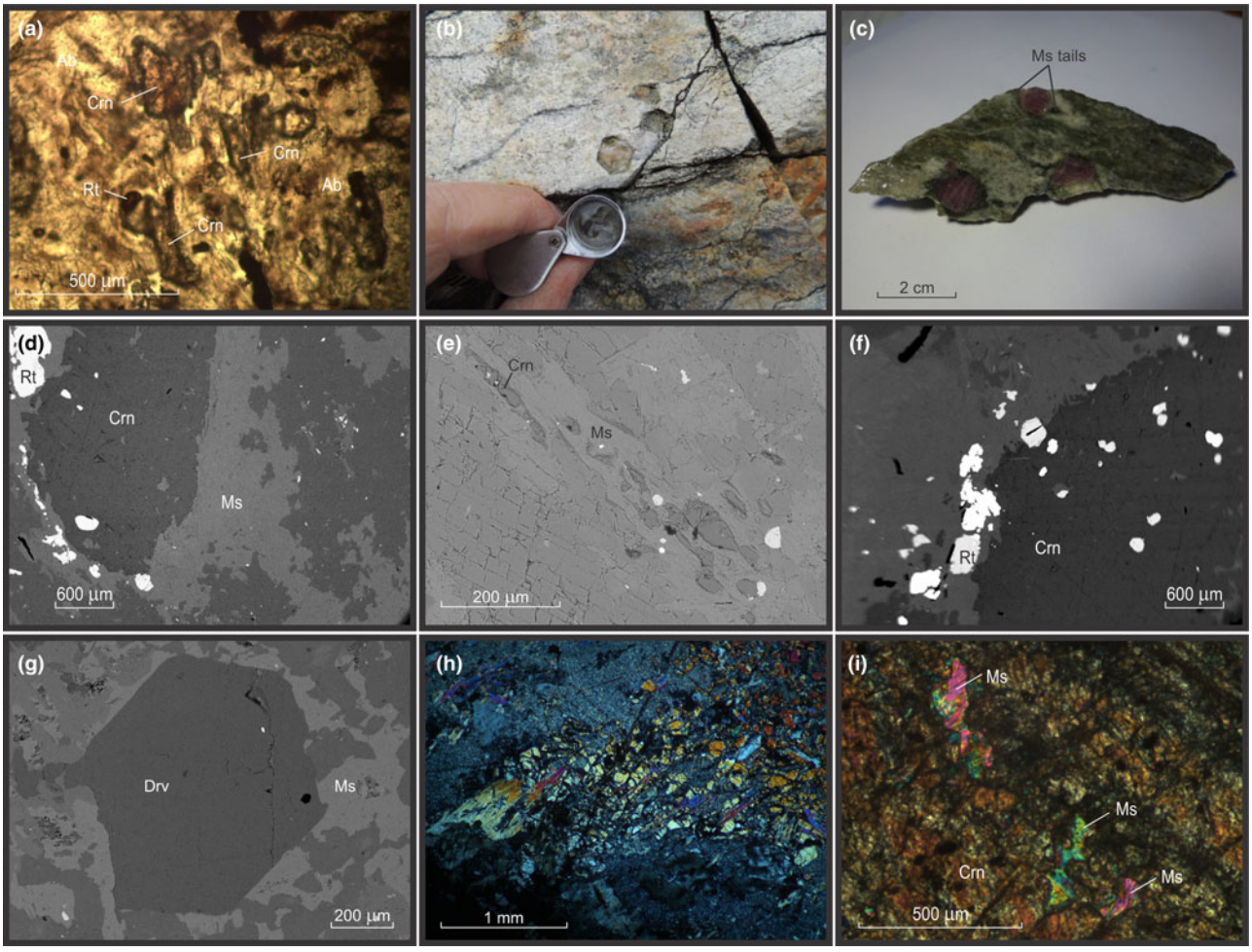

Fig. 2. Images of corundum-bearing feldspathic gneiss, Frenchvale quarry, Cape Breton Island. (*a*) Photomicrograph of fabric-forming corundum crystals (plane polarised light; sample FQ8); (*b*) field photograph of partly fuchsitised corundum porphyroblasts; (*c*) hand sample photograph showing muscovite-rich pressure shadows on corundum porphyroblasts, indicating that they are a pre-kinematic phase; (*d*) BEI of muscovite vein cross-cutting barrel corundum (FQ2); (*e*) BEI of trails of small corundum grains enclosed by fabric-forming muscovite (FG6); (*f*) BEI of rutile inclusions in corundum and in the feldspathic groundmass (FQ2). (*g*) BEI of muscovite-mantled red dravite (FQ6); (*h*) photomicrograph of brown dravite (high relief grains) partly replaced by sericite and fabric-forming muscovite in fuchsitised feldspathic gneiss (crossed nichols; FQ2B); (*i*) photomicrograph of corroded muscovite inclusions in barrel corundum (crossed nichols; FQ25). Abbreviations follow Whitney and Evans (2010): Ab = albite; Crn = corundum; Drv = dravite; Ms = muscovite; Rt = rutile.

(Fig. 3*b*). The brown dravite is typically enclosed and in places replaced largely by muscovite (Fig. 2*h*), and in one sample is cut by a narrow, monazite-(Ce)-bearing calcite vein. In another sample, dravite is enclosed partly by barrel corundum. Both the brown and red dravite have an X_{Mg} ratio of 0.88–0.90 (Table 1). The dravite averages 10 wt.% B_2O_3. The low Ti contents (0.9–1.9 wt.% TiO_2) of biotite in these rocks are consistent with their magnesian compositions (X_{Mg} [= Mg/(Fe + Mg)] ≈0.8–0.9), on the basis of the Ti saturation surface for biotite in medium-pressure metapelites described by Henry *et al.* (2005). Chlorite is only slightly less magnesian (X_{Mg} = 0.77). As will be seen, the unusually high X_{Mg} ratios of these minerals is due to the low bulk iron content of the feldspathic gneiss.

The matrix contains both twinned albite (An_6) and alkali feldspar (microcline). Muscovite is conspicuous in most of the fresh corundum-bearing samples. It occurs as isolated flakes within these rocks, is concentrated in discontinuous bands in part defining gneissosity in the rock, is associated with partly-chloritised biotite, and commonly encloses dravite and corundum. The partial muscovitisation of otherwise fresh (i.e. pink) corundum (Fig. 2*c*) shows that this event is unrelated to late alteration (fuchsitisation) associated spatially with the wide quartz vein in the outcrop (Fig. 1). The muscovite contains up to 2.7 wt.% MgO, and has a Si/Al ratio of about 1.1. Fuchsite formed at the expense of corundum contains ~0.4 wt.% Cr_2O_3, approximately twice the amount of this component occurring in muscovite in these rocks. Feldspars in the fuscitised samples are heavily sericitised.

Relatively fresh, pink corundum occurs well away from the quartz vein, and in the easternmost part of the quarry, between exposures of granodiorite and pegmatite. It contains between 0.7 and 1.0 wt.% Cr_2O_3. Corundum porphyroblasts host abundant stubby rutile inclusions, but networks of slender rutile needles ('silk'; O'Donoghue, 1988) that have been interpreted variously as an exsolved phase or through the epitaxial co-precipitation of both minerals (Palke and Breeding, 2017), were not observed in the Frenchvale quarry rocks. The rutile inclusions are distributed irregularly in these porphyroblasts, although they tend to be concentrated near their margins. They do not define fossil fabrics (oriented inclusion trails). Traces of white mica and biotite are also included by some of these porphyroblasts. The lower-grade

https://doi.org/10.1180/mgm.2018.165 Published online by Cambridge University Press

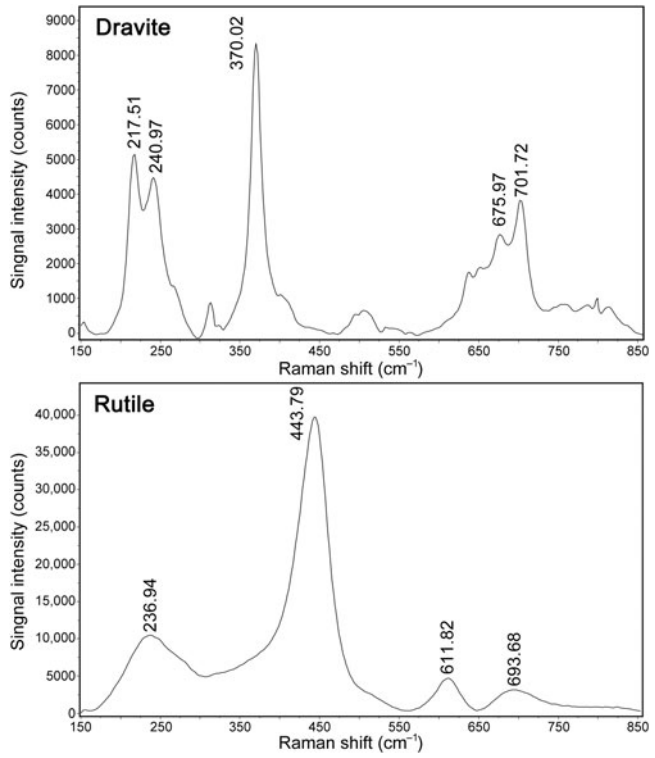

Fig. 3. Raman spectra for rutile and dravite.

counterpart of the feldspathic gneiss is not preserved in Frenchvale quarry, precluding rigorous assessment of the corundum-forming reaction(s), but the presence of trace amounts of corroded muscovite in some barrel-shaped corundum porphyroblasts (Fig. 2*i*) suggests that the corundum formed at the expense of this mineral.

Stubby rutile crystals occur both as inclusions in corundum and in the groundmass, but the included rutile grains tend to be smaller and more rounded than those in the matrix (Fig. 2*f*). The distribution of rutile in the gneiss suggests that the rutile-forming reaction continued during and after corundum nucleation and growth. The paucity of biotite in the groundmass suggests that rutile formed at the expense of this mineral (e.g. Meinhold, 2010). Dravite shows a rimwards increase in Ti (0.4 to 0.7 wt.% TiO_2 across the crystal shown in Fig. 2*g*), suggesting that, like corundum, it also formed during biotite breakdown. The partial inclusion of dravite by barrel corundum porphyroblasts suggests that these minerals are coeval.

The dolomitic marble is a fine grained (~1 mm), granoblastic rock in which foliation is defined by narrow, phlogopite-rich bands. Some samples contain small, isolated patches of calcite. Forsterite, now serpentinised, and diopside occur locally in trace amounts. The coexistence of forsterite and diopside and local occurrence of wollastonite indicates peak metamorphic conditions in the upper amphibolite facies, consistent with the presence of corundum in the feldspathic gneiss.

Narrow (metre-scale) sheets of biotite-hornblende granodiorite and biotite-bearing granitic pegmatite occur sporadically in Frenchvale quarry (Fig. 1). Lithological contacts, including the interface between granitoid rocks and their host, are poorly exposed. The granodiorite is medium grained (~1 mm); biotite crystals are relatively small (~0.2 mm), and are oriented randomly. Feldspars in the granodiorite are moderately to heavily sericitised. Where preserved, plagioclase is normally zoned oligoclase ($An_{26–22}$). Biotite is relatively fresh, but some grains are partly chloritised along cleavage planes. Feldspars in the granitic pegmatite are partly sericitised, but, as in the granodiorite, biotite is relatively fresh. Biotite in these rocks has an X_{Mg} ratio of ~0.4, and contains 3–4 wt.% TiO_2. Hornblende is confined to the granodiorite. It has an X_{Mg} ratio of 0.35–0.39.

Table 1. Representative compositions of minerals from the feldspathic gneiss at Frenchvale quarry*.

	Crn	Kfs	Ab	Bt	Ms	Fcs	Drv	Rt
Wt.%								
SiO_2	bdl	66.19	67.56	37.71	46.06	47.79	40.21	0.86
TiO_2	bdl	0.17	bdl	1.73	0.77	1.41	0.53	98.65
Al_2O_3	99.77	17.99	20.12	19.85	35.27	34.10	35.54	0.36
Cr_2O3	0.82	bdl	bdl	0.19	0.18	0.37	bdl	bdl
FeO	bdl	bdl	bdl	5.41	0.34	0.58	1.98	bdl
MnO	bdl	bdl	bdl	0.03	bdl	bdl	bdl	bdl
MgO	bdl	bdl	bdl	19.24	1.17	0.63	8.22	bdl
CaO	bdl	bdl	1.43	0.13	bdl	bdl	0.16	0.11
Na_2O	bdl	0.53	10.84	0.15	0.54	0.60	2.34	bdl
K_2O	bdl	15.13	0.12	9.99	10.12	10.31	0.00	bdl
B_2O_3	ns	ns	ns	ns	ns	ns	10.3	ns
Total	100.6	100.0	100.1	94.4	94.5	95.8	99.3	100.0
Molar fraction								
X_{Ab}		0.051	0.926					
X_{Mg}				0.864			0.881	

*Mineral abbreviations follow Whitney and Evans (2010); Fcs = fuchsite, bdl = below detection limit, ns = not sought.

Geochemistry

Major, minor and trace elements

Average compositions of the fresh and altered corundum-bearing gneiss, dolomitic marble, granodiorite and granitic pegmatite are given in Table. 2.

The fresh corundum-bearing feldspathic gneiss is dominated by silica (56.9 wt.%) and alumina (26.8 wt.%), with very high alkali contents (7.1 wt.% Na_2O, 3.2 wt.% K_2O) and low femic components (Fe_2O_3+MgO <1 wt.%) and CaO (1.1 wt.%). The substantial titania content (1.1 wt.% TiO_2) reflects the modal abundance of rutile in these rocks. Their high Na_2O content and Na_2O/K_2O ratio (= 2.2) are distinctive, as is their elevated MgO/Fe_2O_3 ratio (= 1.3–2.1), which accounts for the magnesian character of dravite and biotite in these rocks. The bulk compositions of the fresh feldspathic gneiss plot in or near the three-phase Crn–Bt–Drv triangle on an AFM diagram (projected from Kfsp and Ab; Fig. 4). Owing to their high alkali contents, these rocks have distinctive chemical indices of alteration (CIA [Nesbitt and Young, 1982] = 61–70) and weathering (CIW [Harnois, 1988] = 57–64; WIP [Parker, 1970] = 58–67).

In marked contrast to their fresh counterparts, the altered corundum-bearing rocks are enriched in femic components (Fe_2O_3+MgO = 6.8 wt.%) and K_2O (7.2 wt.%) but depleted strongly in CaO (0.4 wt.%) and, particularly, Na_2O (0.1 wt.%). As a result, they have much higher CIA (= 75), CIW (= 97) and WIP (= 95–96) values than the fresh corundum-bearing samples. Their higher LOI content (averaging 5.3 wt.% *vs.* 1.7 wt.%) records the alteration of corundum (fuchsitised) and groundmass feldspars (sericitised) in these samples. The strong depletion in alkalis accounts for their much higher A/CNK (=Al_2O_3/CaO +

https://doi.org/10.1180/mgm.2018.165 Published online by Cambridge University Press

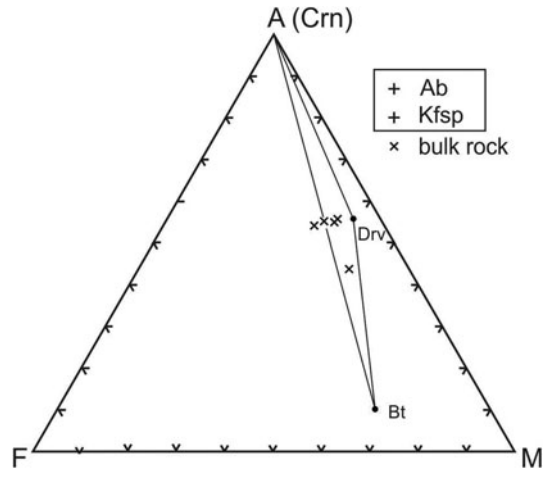

Fig. 4. AFM diagram (projected from K feldspar and albite) showing that the bulk compositions of the corundum-bearing feldspathic gneiss plot in and near the Crn–Bt–Drv field.

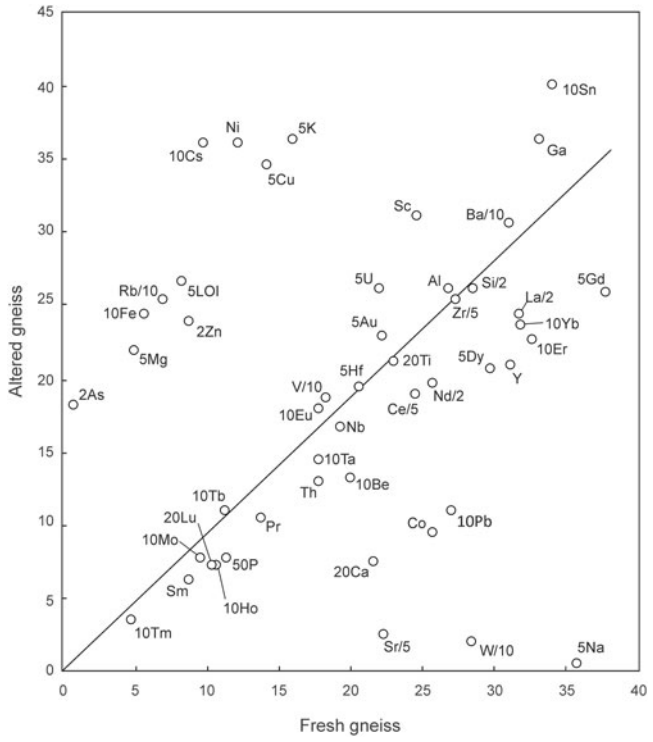

Fig. 5. Isocon diagram (Grant, 2005) comparing the mean compositions of fresh and altered (fuchsitised) feldspathic gneiss from Frenchvale quarry (see text). Data are scaled as indicated. Major element oxides are abbreviated as cations, and are in wt.%. Trace elements are in ppm.

$Na_2O + K_2O$ molecular proportions) ratio (= 3.0 *vs.* 1.56) compared with unaltered samples.

The average compositions of fresh and altered gneiss samples are compared on the isocon diagram (Grant, 2005) shown in Fig. 5. With respect to a best-fit isocon constrained by the concentrations of Ti, Zr and various rare-earth elements (*REEs*), the altered gneiss shows marked enrichment in K, Rb, Fe, Mg, Ni, Cu and volatiles (LOI), and depletion in Na, Ca, Sr, W, Co, Pb, P, Y and several of the *REE*s. Depletion in P, Y and *REE*s suggest the dissolution of phosphate minerals (possibly including apatite, monazite and/or xenotime) during alteration.

Relative to the best-fit isocon, element gains and losses can be quantified using the density of representative samples (fresh gneiss sample GQ15: $\rho = 2.74$ g/cm^3; altered sample FQ5: $\rho = 2.90$ g/cm^3) and the equations presented by Grant (2005). With regard to the alkali- and alkali-earth metals, alteration is consistent with the thorough sericitisation of albite and K feldspar, with extreme depletion in Na (–98%), Ca (–61%), Sr (–88%), and enrichment in white mica components such as K (+142%) and Rb (+291%). Barium, however, increased by only 6%, so this component was essentially retained by the gneiss during sericitisation of K feldspar. As is shown below, some of the same high-field-strength elements (HFSE) used to define the best-fit isocon in Fig. 5 occur in PAAS (post-Archean Australian shale)-like concentrations in the feldspathic gneiss, suggesting that the protolith of this rock was a very fine grained, clay-rich clastic sediment.

Apart from minor amounts of SiO_2 (1.8 wt.%) and Al_2O_3 (0.5 wt.%), the dolomitic marble is rather pure, with 22.1 wt.% MgO, 29.7 wt.% CaO and LOI (presumably mostly CO_2) of 45.5 wt.%, consistent with the presence of only minor amounts of silicate minerals.

Evidently due to the effects of seritisation, the granodiorite is mildly peraluminous (A/CNK = 1.1; Table 2) despite containing calcic amphibole; the granitic pegmatite is even more so (A/CNK = 1.23). Regardless of being partly sericitised, the pegmatite is considerably more sodic than the granodiorite (Na_2O/K_2O = 5.3 *vs.* 1.1).

The presence of albite and magnesian composition of biotite and dravite in the gneiss reflect the unusual bulk composition of these rocks, ascribed here (see below) to a sedimentary environment (offshore fluvial deposits) and diagenesis (albitisation).

Oxygen isotopes

Eight representative samples were analysed for their bulk oxygen isotope composition. The isotopic composition of individual corundum crystals – though widely reported in the literature (e.g. Giuliani *et al.* 2005) – were not determined separately owing to the abundance of rutile crystals entrained in them (Fig. 2*d*,*f*). The specimens analysed (Table 3) consist of: three samples of fresh-corundum-bearing feldspathic gneiss (FQ6, FQ8, FQ26); one partly (FQ5); and two thoroughly fuchsitised (FQ2, FQ4) feldspathic gneisses; granodiorite (FQ24); and the 1.2 m wide quartz vein (FQ1B) to which the fuchsitised gneisses are associated spatially. The fresh-corundum-bearing samples have isotopic ratios ($\delta^{18}O_{VSMOW}$ values = 8.1 to 10.7‰) that overlap those of the fuchsitised samples ($\delta^{18}O_{VSMOW}$ values = 6.7 to 11.2‰). The altered sample with the highest $\delta^{18}O$ was collected closest to the quartz vein, which has the same $\delta^{18}O_{VSMOW}$ value (11.2‰). The granodiorite has the highest $\delta^{18}O_{VSMOW}$ value (12.1‰) of all analysed samples.

Fluid-inclusion microthermometry

In samples from the quartz vein (FQ29), two main fluid-inclusion types were identified on the basis of petrographic and microthermometric properties: (1) Type 1, two-phase, aqueous-carbonic (H_2O-NaCl + CO_2 + CH_4 ± N_2) inclusions hosted in clusters of indeterminate origin in quartz and range in size from 4–9 μm (Fig. 6*a*); and (2) Type 2, one-phase, low density CH_4-only inclusions hosted along healed planes and fractures of secondary and pseudosecondary origin (Fig. 6*b*). Type 1 inclusions appear to

https://doi.org/10.1180/mgm.2018.165 Published online by Cambridge University Press

Table 2. Average major-, minor- and trace-element composition of paragneisses (marble, feldspathic gneiss) and granitoid rocks at Frenchvale quarry.

	Marble ($n = 6$)	Fresh Fsp gneiss (5)	Alt Fsp gneiss (3)	Granite (3)	Pegmatite (2)
Wt.%					
SiO_2	1.8	56.9	52.4	62.7	59.1
TiO_2	bdl	1.1	1.1	0.9	0.2
Al_2O_3	0.5	26.8	26.2	16.3	23.3
Fe_2O_3	0.3	0.6	2.4	5.6	1.0
MnO	0.0	bdl	bdl	0.1	bdl
MgO	22.1	1.0	4.4	2.0	1.4
CaO	29.7	1.1	0.4	2.9	2.6
Na_2O	bdl	7.1	0.1	3.7	7.7
K_2O	bdl	3.2	7.2	3.3	1.5
P_2O_5	bdl	0.2	0.2	0.3	0.3
Cr_2O_3	bdl	bdl	bdl	bdl	bdl
LOI	45.5	1.7	5.3	1.9	2.8
Total	99.9	99.8	99.8	99.7	99.8
TOT/C	12.4	0.1	0.1	bdl	0.1
TOT/S	bdl	bdl	bdl	bdl	0.1
ppm					
Ni	bdl	12.2	36.0	bdl	bdl
Sc	bdl	24.6	31.0	16.0	8.0
Ba	6.0	310.4	306.7	871.7	175.5
Be	bdl	2.0	1.3	3.3	7.0
Co	2.7	25.7	9.4	46.2	23.8
Cs	0.1	1.0	3.6	2.5	2.2
Ga	0.1	33.1	36.4	19.2	33.4
Hf	0.1	4.1	3.9	9.0	2.0
Nb	0.6	19.3	16.7	22.1	8.2
Rb	1.6	69.7	253.4	94.9	48.6
Sn	bdl	3.4	4.0	1.7	0.5
Sr	119.7	111.4	12.9	284.5	755.7
Ta	bdl	1.8	1.3	1.4	1.3
Th	0.3	17.8	14.5	15.0	11.2
U	2.1	4.4	5.2	3.6	4.7
Mo	0.2	1.0	0.7	0.7	5.7
Cu	1.2	2.8	6.9	8.1	9.0
Pb	93.1	2.7	1.1	5.1	1.5
Zn	98.8	4.4	12.0	36.7	2.5
Ni	1.2	15.1	37.4	3.8	11.5
As	0.1	0.4	9.1	0.7	bdl
Cd	0.2	bdl	bdl	bdl	bdl
Sb	bdl	bdl	0.1	bdl	bdl
Bi	bdl	bdl	bdl	0.1	0.1
Ag	bdl	bdl	bdl	bdl	bdl
Au	1.3	4.4	4.6	20.1	1.8
Hg	bdl	0.1	bdl	bdl	0.1
Tl	bdl	bdl	bdl	0.2	bdl
Se	bdl	bdl	bdl	bdl	bdl
V	1.8	182.6	186.7	61.7	35.5
W	20.1	284.4	21.1	341.4	122.1
Zr	7.4	136.4	126.7	388.5	61.1
Y	1.7	31.1	20.8	41.1	18.7
La	2.8	63.4	48.7	37.7	20.3
Ce	5.2	122.4	95.1	79.4	37.8
Pr	0.5	13.7	10.6	10.1	4.5
Nd	2.1	51.5	39.3	39.9	17.8
Sm	0.3	8.8	6.3	8.4	3.4
Eu	0.1	1.8	1.8	2.1	1.3
Gd	0.3	7.5	5.2	8.0	3.3
Tb	bdl	1.1	0.7	1.3	0.5
Dy	0.3	5.9	4.1	7.6	3.0
Ho	0.1	1.1	0.8	1.6	0.6
Er	0.2	3.3	2.3	4.7	1.8
Tm	bdl	0.5	0.4	0.7	0.3
Yb	0.2	3.2	2.4	4.5	1.6
Lu	bdl	0.5	0.4	0.7	0.2

also be hosted in secondary inclusion trails crosscutting quartz grain boundaries (Fig. 6c), however, inclusions hosted in these

Table 3. Whole-rock oxygen isotopic data for various rock types from Frenchvale quarry.

Sample ID	$\delta^{18}O$‰ *vs.* VSMOW	Lithology	Distance (m)*
FQ1B	11.8	Quartz	0
FQ2	11.2	Alt. Fsp. Gneiss	1.2
FQ4	7.8	Alt. Fsp. Gneiss	2.6
FQ5	6.7	Partly alt. Fsp gneiss	3.5
FQ6	10.4	Fsp gneiss	7.6
FQ8	10.7	Fsp gneiss	19
FQ26	8.1	Fsp gneiss	>50
FQ24	12.1	Granodiorite	>50

*From quartz vein.

secondary trails are typically too small or have been decrepitated and/or modified making accurate microthermometric analysis impossible. Type 1 inclusions can be divided into two subtypes based on salinity (Fig. 7), as they share identical petrographic properties. Type 1A inclusions are of low salinity (4 wt.% NaCl equiv.; $n = 12$) and homogenize at 208 ± 36°C ($n = 9$, while Type 1B inclusions are of intermediate salinity (13.2 wt.% NaCl equiv.; $n = 5$) and homogenize at 200°C ($n = 1$). Variations in salinity might represent temporally-distinct pulses of fluids with unique origins but interpretation is limited by similar petrographic characteristics and poor representation in the samples investigated.

Laser Raman microspectroscopy

Laser Raman microspectroscopy can identify the presence of gas phases (e.g. CO_2, N_2, CH_4) otherwise unidentifiable by traditional microthermometric techniques. Two-phase Type 1 fluid-inclusion vapour bubbles contain an average ($n = 2$) of 50.8 ± 5.4 mol.% CO_2, 44.8 ± 5.5 mol.% CH_4 and 4.4 ± 0.1 mol.% N_2. One-phase Type 2 fluid inclusions contain low density CH_4 with variable N_2. No water or CO_2 were detected in Type 2 inclusions. When N_2 does occur, it averages ($n = 2$) 31.4 ± 0.8 mol.%, with the remainder consisting of CH_4.

Gas chromatography

A euhedral crystal of quartz from vein sample FQ29 was fragmented, cleaned and weighed for analysis. The bulk fluid (Fig. 8) is water dominated (99.60 mol.% H_2O) with minor methane (0.256 mol.%) and carbon dioxide (0.14 mol.%), and traces of C_{2+} hydrocarbons (0.003 mol.%; ethane, propane, 1-propene, butane). Considering only carbonic species, the bulk fluid possesses a composition of 34.5 mol.% CO_2, 64.7 mol.% CH_4 and 0.8 mol.% C_{2+} hydrocarbons. Due to the nature of the analytical GC column, nitrogen and carbon monoxide co-elute with methane and carbon dioxide, respectively, and thus could not be quantified via gas chromatography.

Discussion

Giuliani *et al.* (2014) distinguished two main categories of gem corundum deposits: (1) magmatic deposits, including (*a*) those hosted by mafic/ultramafic rocks but genetically related to granitoid magmatism and/or hydrothermal activity, and (*b*) those hosted by alkali basalt and mafic dykes; and (2) metamorphic deposits formed from marine sediment protoliths (carbonate platformal rocks). Type 2 deposits consist of marble-hosted sapphire

https://doi.org/10.1180/mgm.2018.165 Published online by Cambridge University Press

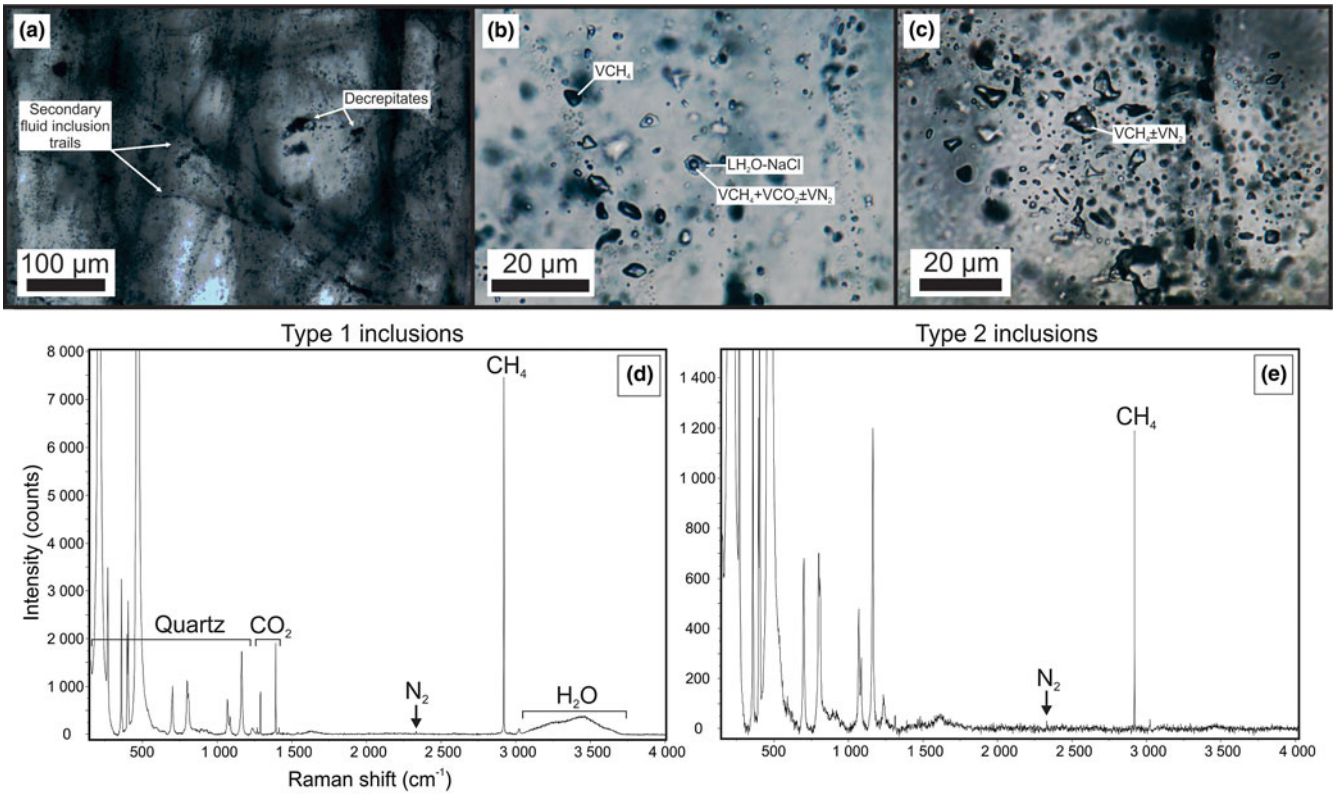

Fig. 6. Fluid-inclusion photomicrographs and associated Raman spectra from vein sample FQ29. (*a*) Heavily decrepitated quartz with abundant secondary fluid inclusion trails. (*b*) Two-phase Type 1 (H_2O–NaCl + CO_2 + CH_4 ± N_2) inclusions adjacent to a secondary trail of mono-phase Type 2 (CH_4 ± N_2) inclusions. (*c*) A plane of mono-phase Type 2 inclusions. (*d*) Raman spectra of the vapour bubble in a Type 1 inclusion displaying the presence of H_2O, CO_2, CH_4 and minor N_2. (*e*) Raman spectra of a mono-phase Type 2 inclusion displaying CH_4 and minor N_2.

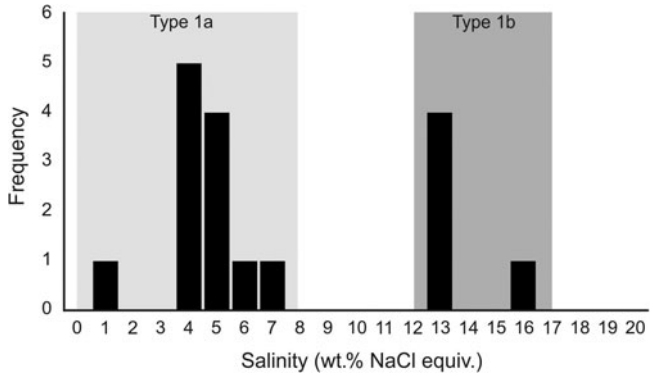

Fig. 7. Fluid-inclusion salinity histogram illustrating the two subtypes of two-phase Type 1 (H_2O–NaCl + CO_2 + CH_4 ± N_2) inclusions. Type 1A inclusions are of low salinity (4 wt.% NaCl equiv.; n = 12) and homogenise at 208 ± 36°C (n = 9, while Type 1B inclusions are of intermediate salinity (13.2 wt.% NaCl equiv.; n = 5) and homogenise at 200°C (n = 1).

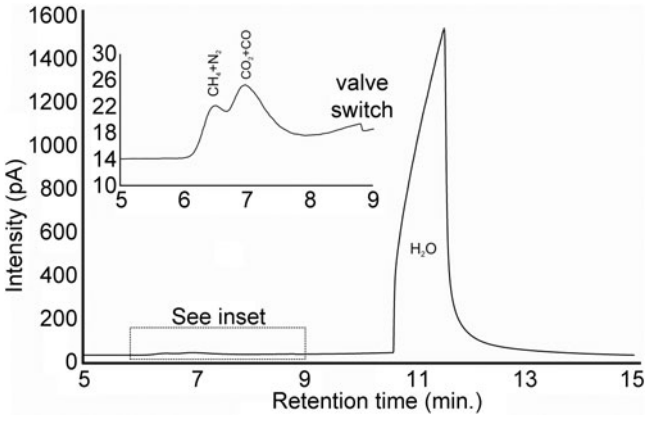

Fig. 8. Bulk volatile gas chromatogram of quartz from vein sample FQ29. The bulk fluid is water-dominated (99.60 mol.% H_2O) with minor methane (0.256 mol.%) and carbon dioxide (0.14 mol.%).

and ruby. The Cape Breton occurrence is a variation of Type 2 deposits, differing in the fact that the corundum occurs in highly aluminous feldspathic gneiss associated spatially with dolomitic marble. On the basis of our observations no corundum occurs in the marble itself. The corundum-bearing samples contain on average only 1.1% CaO.

Assuming that the feldspathic gneiss is part of the same sedimentary sequence as the dolomitic marble, its protolith was some type of supracrustal rock. The fresh corundum-bearing samples, however, have unusual compositions that, if unmodified since the deposition of their protolith, match few if any unaltered sedimentary rocks. In terms of their silica and alumina contents, however, they resemble particulate matter from various rivers, notably the Congo (58 wt.% SiO_2, 25 wt.% Al_2O_3; see table 2.8 in Taylor and McLennan, 1985), but they are substantially depleted in Fe and enriched in alkalis, especially Na. Indeed, spider diagrams depicting the absolute concentrations of various components in suspended sediment in several west-African Rivers, including the Congo, show negative anomalies for Na (and Sr), suggesting that the continental crustal rocks in their drainage basins had

https://doi.org/10.1180/mgm.2018.165 Published online by Cambridge University Press

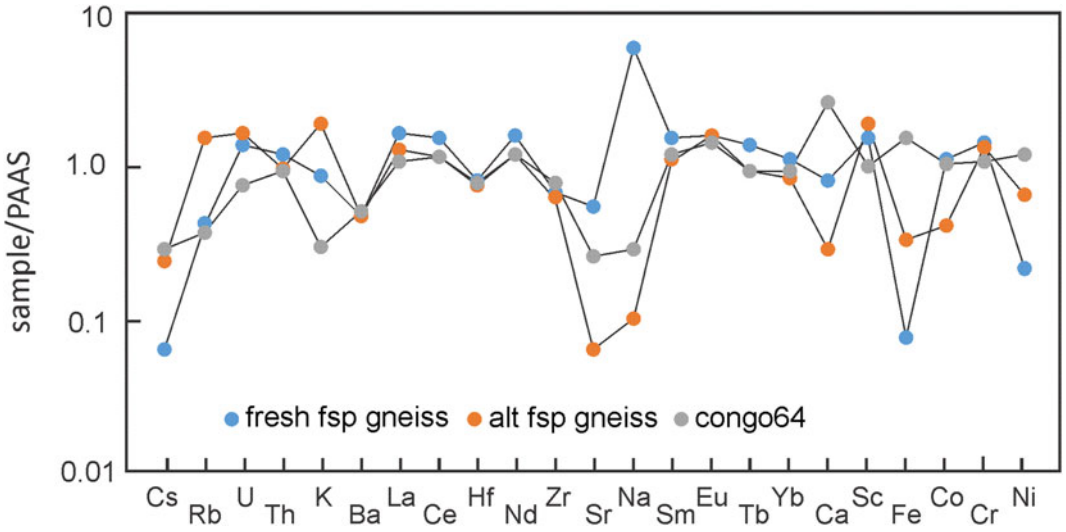

Fig. 9. PAAS-normalised spider diagram comparing the mean composition of the fresh and altered (fuchsitised) corundum-bearing feldspathic gneiss with a fine sediment from the Congo River (Dupré *et al.*, 1996). Normalising data are from Taylor and McClennan (1985).

been depleted previously in these components by ancient chemical weathering events (i.e. that the source rocks of these sediments include shale or shale-derived granitoid rocks; Gaillardet *et al.*, 1995). Notwithstanding its suspended sediment load, the Congo – the world's second largest river system – has a very low load of dissolved inorganic components (Spencer *et al.*, 1999).

The mean compositions of fresh and altered (fuchsitised) feldspathic gneiss are compared with fine suspended sediment from the Congo River (sample Congo64; Gaillardet *et al.*, 1995) on a PAAS-normalised plot shown in Fig. 9. These samples have PAAS-like concentrations of various radionuclides (U, Th), HFSE (Hf, Zr, selected *REE*s), and transition metals (Co, Cr and Ni). All three, especially the fresh feldspathic gneiss, are depleted in Cs compared with PAAS, and only the altered gneiss has higher K concentrations than PAAS. As noted earlier, the fresh gneiss is enriched significantly (and altered gneiss depleted) in Na, and both are depleted in Fe. The altered gneiss is also depleted in plagioclase components (Ca, Sr). The PAAS-like concentrations of relatively immobile components (HFSE) in the feldspathic gneiss indicate derivation from altered (albitised), iron-poor, fine-grained, clay-rich sediments. These evidently were deposited in a marine basin in which dolomitised lime muds were accumulating. This provides a possible explanation for the Fe-poor composition of the feldspathic gneiss: regardless of grain size, clastic sediments accumulating in distal parts of large fluvial systems can be depleted in Fe oxides owing to the flocculation and hence preferential deposition of phyllosilicates farther inshore (Poulton, 1999). Evidently this process, though effective in depleting the sediment load in Fe oxides, allowed clay-group minerals to be transported to the carbonate platform.

Albitisation is a widespread phenomenon in upper crustal rocks, and can be related to the diagenesis of sediments, deuteric alteration of granitoid rocks, alteration adjacent to (per)alkaline intrusions, and the ductile deformation and exhumation of metamorphic terrains (Boulvais *et al.*, 2007, and references therein). In some instances, albitisation can involve surface waters (McLelland *et al.*, 2002), and it can be associated with desilication/dequartzification; the opposite effect can be associated with potassic metasomatism. Owing to early albitisation of their protoliths, high-grade metasediments – even granulites – can contain albite rather than more calcic plagioclase (Owen *et al.*, 2003).

There are no known alkaline intrusions or major mylonite zones near Frenchvale quarry, effectively excluding igneous or tectonic activity as the cause of wholesale Na-enrichment recorded by the composition of the feldspathic gneisses at this locality. A granitic pegmatite occurring sporadically at Frenchvale quarry is sodic in composition, but owing to its small volume (based on outcrop distribution) seems an implausible source of Na-metasomatic fluids responsible for sodic alteration of the feldspathic rocks. Indeed, it could be argued that interaction of pegmatitic fluids with the sodic gneiss accounts for this aspect of their composition (cf. Owen and Greenough, 1999). Rather, diagenetic albitisation of detrital clays in the sedimentary protolith is a more viable process. This accounts for the quartz-free character of the feldspathic gneiss insofar as the transformation of detrital clays such as illite to albite would consume modal quartz. Residual aluminous phyllosilicates surviving this process could then ultimately, after reaction to a higher temperature phase (evidently muscovite given its local occurrence as a relict, included phase in barrel corundum), be converted to corundum during subsequent metamorphism. The occurrence of small, partly corroded, fabric-forming corundum and of lozenge-shaped muscovite tails on their larger, barrel-shaped counterparts points to metamorphism culminating in high-strain events. The coeval formation of rutile in the feldspathic gneiss and of zircon in granodiorite, suggests that magmatism preceded or accompanied deformation at ~560 Ma (Hopkins *et al.*, 2017).

Owing to the relatively narrow total range in $\delta^{18}O_{VSMOW}$ values in the samples, a lack of systematic differences between samples of varied alteration intensity or proximity to quartz veining, and in the absence of mineral-specific isotope data, the data reported in Table 3 provide only limited constraints on aspects of the geochemical history of the feldspathic gneiss. The narrow range in $\delta^{18}O_{VSMOW}$ for rocks deemed altered, partly altered, and 'fresh' is not consistent with interaction with an external fluid at a high fluid:rock ratio. Further evaluation of equilibrating fluid sources requires mineral isotope data to first assess the degree of internal O isotope equilibrium in the rocks.

https://doi.org/10.1180/mgm.2018.165 Published online by Cambridge University Press

Although the narrow sheets of granodiorite might have played a role in the late metamorphic history of the feldspathic gneiss, as suggested by the presence of coeval (560 Ma) rutile in both rocks (Hopkins *et al.*, 2017), the very low silica content of the dolomitic marble (1.7% SiO_2) and low lime content of the feldspathic gneiss (1.1% CaO) suggest that these paragneissic host rocks have not been appreciably skarned. Rather, the data presented here suggest that sodic alteration occurred early in the sedimentary history of the protolith of the feldspathic gneiss (during diagenesis).

The quartz vein cutting the feldspathic gneiss preserves water-rich (99.60 mol.% H_2O) fluid inclusions that evidently are responsible for the local (metre-scale) fuchsitisation of corundum. Emplacement of the quartz vein and fuchsitisation associated with it post-date the partial greenschist-facies retrogression of these rocks. The source of minor CO_2 and CH_4 in the water-rich fluid hosted in temporally-late pseudosecondary and secondary fluid-inclusion trails in the quartz vein cutting the gneiss remains unclear. The carbon dioxide might be of metamorphic origin, having migrated from depth through fault conduit systems, or sourced more locally from the decarbonation of the nearby marble. The methane might also be sourced locally as a result of the reduction of CO_2 via H_2 gas released during the serpentinisation of olivine in dolomitic marble units, or through the re-speciation of CO_2 through the interaction with graphitic units. However, it is interpreted that the presence of minor CO_2 and CH_4 had little if any influence on alteration.

As noted by Mossman *et al.* (2007), the Frenchvale quarry corundum occurrence is a product of regional rather than contact metamorphism. The mineralogy and geochemistry of these rocks show that they are not skarns. Rather, they are a distinct category of carbonate-rock-*associated* corundum deposit.

Conclusions

The Frenchvale quarry corundum-bearing rocks are a variant of Type 2 (metamorphic/metasomatic) sapphire and ruby deposits. Instead of being hosted by metacarbonate rocks, however, the corundum occurs in feldspathic gneiss that is associated spatially with dolomitic marble. The protolith of the gneiss is interpreted on geochemical grounds to have been a fine clastic fluvial sediment deposited offshore on a carbonate platform. Their Fe-poor composition, responsible for the highly magnesian composition of biotite and dravite in the gneiss, is interpreted as a primary feature of these distal sediments, but their sodic character is interpreted as a product of diagenetic albitisation. The corundum formed in the upper amphibolite facies prior to a late, passive, greenschist-facies overprint that partly masks the earlier, higher-grade metamorphic history of the feldspathic gneiss. There is no evidence that the oxygen isotopic signature of the gneisses has been modified pervasively by an externally derived magmatic or metamorphic fluid, even where intruded by narrow granodiorite sheets. Although we cannot discount the possible role of contact metamorphism in the formation of the corundum, at least on a scale larger than individual minor intrusions in the quarry, the composition and mineralogy of these rocks shows that they are not skarns *sensu stricto*.

Acknowledgements. This investigation was supported by a Saint Mary's University Faculty of Graduate Studies and Research grant to the first author. The manuscript benefited from incisive comments by Chris Harris and Dave Waters.

References

Barr S.M. (1990) Granitoid rocks and terrane characterization: An example from the northern Appalachian Orogen. *Geological Journal*, **25**, 295–304.

Barr S.M., Kamo S. and White C.E. (1999) A late Neoproterozoic age for a tonalite dyke in the Boisdale Hills, Cape Breton Island, Nova Scotia. *Atlantic Geology*, **35**, 197–202.

Beeskow B., Rankin A.H., Murphy P.J. and Treloar P.J. (2005) Mixed CH_4-CO_2 fluid inclusions in quartz from the South Wales Coalfield as suitable natural calibration standards for microthermometry and Raman spectroscopy. *Chemical Geology*, **223**, 3–15.

Bodnar R.J. (2003) Introduction to fluid inclusions. Pp. 1–8 in: *Fluid Inclusions: Analysis and Interpretation* (I. Samson, A. Anderson and M. Marshall, editors). Mineralogical Association of Canada, Short Course, **32**.

Boulvais P., Ruffet G., Cornichet J. and Mermet M. (2007) Cretaceous albitization and dequartzification of Hercynian peraluminous granite in the Salvezines Massif (French Pyrénées). *Lithos*, **93**, 89–106.

Bray C.J. and Spooner E.T.C. (1992) Fluid inclusion volatile analysis by gas chromatography with photoionization/micro-thermal conductivity detectors: Applications to magmatic MoS_2 and other H_20-CO_2 and H_20-CH_4 fluids. *Geochimica et Cosmochimica Acta*, **56**, 261–272.

Burke E.A. (2001) Raman microspectrometry of fluid inclusions: *Lithos*, **55**, 139–158.

Clayton R.N. and Mayeda T.K. (1963) The use of bromine pentafluoride in the extraction of oxygen from oxides and silicates for isotopic analysis. *Geochimica et Cosmochimica Acta*, **27**, 43–52.

Dubessy J., Poty B., and Ramboz C. (1989) Advances in C-O-H-N-S fluid geochemistry based on micro-Raman spectrometric analysis of fluid inclusions. *European Journal of Mineralogy*, **1**, 517–534.

Dunham A.C. and Wilkinson F.C.F. (1978) Accuracy, precision and detection limits of energy dispersive electron-microprobe analysis of silicates. *X-Ray Spectrometry*, **7**, 50–56.

Dupré B., Gaillardet J., Rousseau D., and Allègre C.J. (1996) Major and trace elements of river-borne material: The Congo Basin. *Geochimica Cosmochimica Acta*, **60**, 1301–1321.

Dzikowski T.J. (2004) *A Comparative Study of the Origin of Carbonate-Hosted Gem Corundum Deposits in Canada*. PhD Dissertation, University of British Columbia, Canada, 259 pp.

Fagan A.J. and Groat L.A. (2014) The geology of the Aappaluttoq ruby and pink sapphire deposit, SW Greenland. *Geological Society of America Abstracts with Programs*, **46**(6). Vancouver, British Columbia, Canada, 19–22 October, 417.

Gaillardet J., Dupré C. and Allegre C.J. (1995) A global mass budget applied to the Congo Basin Rivers: erosion rates and continental composition. *Geochimica Cosmochimica Acta*, **59**, 3469–3485.

Giuliani G., Fallick A.E., Garnier V., France-Lanord C., Ohnenstetter D. and Schwarz D. (2005) Oxygen isotope composition as a tracer for the origins of rubies and sapphires. *Geology*, **33**, 249–252.

Giuliani G., Ohnenstetter D., Fallick A.E., Groat L. and Fagan A.J. (2014) The geology and genesis of gem corundum deposits. Pp. 29–112 in: *The Geology of Gem Deposits* (L. Groat, editor). Mineralogical Association of Canada, vol. **2**.

Goldstein R.H. and Reynolds T.J. (1994) Fluid inclusion microthermometry. Pp. 87–122 in: *Systematics of Fluid Inclusions in Diagenetic Minerals* (R.H. Goldstein and T.J. Reynolds, editors). Society for Sedimentary Geology, Short Course Volume, **31**.

Grant J.A. (2005) Isocon analysis: a brief review of the method and applications. *Physics and Chemistry of the Earth*, **30**, 997–1004.

Harlow G.E. and Bender W. (2013) A study of ruby (corundum) compositions from the Mogok belt, Myanmar: Searching for geochemical fingerprints. *American Mineralogist*, **98**, 1120–1132.

Harnois L. (1988) The CIW: a new chemical index of weathering. *Sedimentary Geology*, **55**, 319–322.

Henry D.J., Guidotti C.V. and Thomson J.A. (2005) The Ti-saturation surface for low-to-medium pressure metapelitic biotites: Implications for geothermometry and Ti-substitution mechanisms. *American Mineralogist*, **90**, 316–328.

https://doi.org/10.1180/mgm.2018.165 Published online by Cambridge University Press

Hopkins R., van Rooyen D., McFarlane C. and Boucher B. (2017) Rutile and zircon LA-ICP-MS U-Pb dating of a corundum-bearing skarn deposit, Frenchvale, Cape Breton Island. *Atlantic Geoscience Society, Program with Abstracts*. Fredericton, NB, Canada, p. 33.

Kerr M.J., Hanley J., Morrison G., Everest J. and Bray C. (2015) Preliminary evolution of hydrocarbon speciation and abundance as an exploration tool for Footwall-style sulfide ores associated with the Sudbury Igneous Complex, Ontario, Canada. *Economic Geology*, **110**, 531–556.

King M.S. and Barr S.M. (2002) The Mira – Bras d'Or terrane boundary in Cape Breton Island, Nova Scotia: potential field and petrophysical investigations applied to tectonic analysis in the northern Appalachian orogeny. *Atlantic Geology*, **38**, 89.

Levinson A.A. and Cook F.A. (1994) Gem corundum in alkali basalt: origin and occurrence. *Gems & Gemology*, **Winter 1994**, 253–262.

McLelland J., Morrison J., Selleck B., Cunningham B., Olson C., Schmidt K. (2002) Hydrothermal alteration of late- to post-tectonic Lyon Mountain Granitic Gneiss, Adirondack Mountains, New York: Origin of quartz–sillimanite segregations, quartz – albite lithologies, and associated Kiruna-type low-Ti Fe-oxide deposits. *Journal of Metamorphic Geology*, **20**, 175–190.

Meinert L.D. (1992) Skarns and skarn deposits. *Geoscience Canada*, **19**, 145–162.

Meinhold G. (2010) Rutile and its applications in earth science. *Earth Science Reviews*, **102**, 1–28.

Mossman D.J., Duivenvoorden J.D. and Isenor F.M. (2007) Cape Breton ruby, a new Canadian gemstone discovery, Cape Breton Island, Nova Scotia. *Journal of Gemmology*, **30**, 279–286.

Nesbitt H.W. and Young G.M. (1982) Early Proterozoic climates and plate motions inferred from major element chemistry of lutites. *Nature*, **299**, 715–717.

O'Donoghue M. (1988) *Gemstones*. Chapman and Hall, London.

Okrusch M., Bunch T.E. and Bank H. (1976) Paragenesis and petrogenesis of a corundum-bearing marble at Hunza (Kashmir). *Mineralium Deposita*, **11**, 278–297.

Owen J.V. and Greenough J.D. 1999. Scapolite pegmatite from the Minas fault, Nova Scotia: tangible manifestation of Carboniferous, evaporite-derived hydrothermal fluids in the western Cobequid highlands? *Mineralogical Magazine*, **63**, 387–397.

Owen J.V., Longstaffe F.J. and Greenough J.D. (2003) Petrology of sapphirine granulite and associated sodic gneisses from the Indian Head Range, Newfoundland. *Lithos*, **68**, 91–114.

Parker A. (1970) An index of weathering for silicate rocks. *Geological Magazine*, **107**, 501–504.

Palke A.C. and Breeding C.M. (2017) The origin of needle-like rutile inclusions in natural gem corundum: a combined EPMA, LA-ICP-MS, and nanoSIMS investigation. *American Mineralogist*, **102**, 1451–1461.

Poulton S.W. (1999) Surface area, iron oxide and organic carbon relationships in sediments. Pp. 279–282 in: *Geochemistry of the Earth's Surface* (H. Armannsson, editor). Balkema, Rotterdam.

Pêcher A., Guiliani G., Garnier V., Maluski H., Kausar A.B., Malik R.H. and Muntaz H.R. (2002) Geology, geochemistry and Ar-Ar geochronology of the Nangimali ruby deposit, Nanga Parbat Himalaya (Azad Kashmir, Pakistan). *Journal of Asian Earth Sciences*, **21**, 265–282.

Raeside R.P. (1989) Geology of the metamorphic rocks of the Boisdale Hills, Cape Breton Island. *Nova Scotia Department of Mines and Energy, Report*, **89–3**, 145–148.

Raeside R.P. and Barr S.M. (1990) Geology and tectonic development of the Bras d'Or suspect terrane, Cape Breton Island, Nova Scotia. *Canadian Journal of Earth Sciences*, **27**, 1371–1381.

Roedder E. (1984) *Fluid inclusions*. Reviews in Mineralogy, **12**. Mineralogical Society of America, Washington, DC, pp. 644.

Salvi S. and Williams-Jones A.E. (1997) Fischer-Tropsch synthesis of hydrocarbons during sub-solidus alteration of the Strange Lake peralkaline granite, Quebec/Labrador, Canada. *Geochimica et Cosmochimica Acta*, **61**, 83–99.

Spencer R.G.M., Stubbins A. and Gaillardet J. (1999) Geochemistry of the Congo River, basin and plume. Pp.554–583 in *Biogeochemical Dynamics at Major River-Coastal Interfaces: Linkages with Global Change* (T.S. Bianchi, M.A. Allison and W.J. Cai, editors). Cambridge University Press, UK.

Sutherland F.L., Hoskin P.W.O., Fanning C.M. and Coenraads R.P. (1998) Models of corundum origin from alkali basaltic terrains: a reappraisal. *Contributions to Mineralogy and Petrology*, **133**, 356–372.

Taylor S.R. and McClennan S. (1985) *The Continental Crust: Its Composition and Evolution*. Blackwell Scientific Publications, Palo Alto, CA.

White C.E., Barr S.J., Davis D.W., Swanton D.S., Ketchum J.W.F. and Reynolds P.H. (2016) Field relations, age, and tectonic setting of metamorphic and plutonic rocks in the Creignish Hills – North Mountain area, southwestern Cape Breton Island, Nova Scotia, Canada. *Atlantic Geology*, **52**, 37–59.

Whitney D.L. and Evans B.W. (2010) Abbreviations for names of rock-forming minerals. *American Mineralogist*, **95**, 185–187.

Wopenka B. and Pasteris J.D. (1986) Limitations to quantitative analysis of fluid inclusions in geological samples by laser Raman microprobe spectroscopy: *Applied Spectroscopy*, **24**, 144–151.

Wopenka B. and Pasteris J.D. (1987) Raman intensities and detection limits of geochemically relevant gas mixtures for a laser Raman microprobe. *Analytical Chemistry*, **59**, 2165–2170.

Yakymchuk C. and Szilas K. (2017) Corundum formation by metasomatic reactions in Archean metapelite, SW Greenland: Exploration vectors for ruby deposits within high-grade greenstone belts. *Geoscience Frontiers*, **9**, 727–749.

https://doi.org/10.1180/mgm.2018.165 Published online by Cambridge University Press